Multimodal distribution of amplitudes of miniature and spontaneous EPSPs recorded in rat trigeminal motoneurones

Ming-Yuan Min and Kwabena Appenteng

Department of Physiology, University of Leeds, Leeds LS2 9NQ, UK

1. The whole-cell variant of the patch recording method has been used to obtain voltage recordings from trigeminal motoneurones in tissue slices (500 μm thick) taken from rats aged 8 days. Membrane properties (input resistance, membrane time constant and rheobase, i.e. threshold current required to elicit an action potential) of the motoneurones were determined and recordings made of the (untriggered) EPSP activity.

2. Untriggered EPSP activity was recorded in standard artificial cerebrospinal fluid (ACSF), ACSF with added tetrodotoxin (TTX) and in nominally Ca^{2+}-free ACSF with added TTX. In each case the amplitude distributions of single EPSPs were peaky and could be fitted by a model consisting of the sum of equidistant Gaussians ($n = 7/9$ cells). In contrast, the amplitude distribution of the noise was always unimodal.

3. All EPSP activity recorded in the presence of TTX was abolished by addition of 6-cyano-7-nitroquinoxaline-2-3-dione (CNQX; 10 μM), suggesting the activity was all mediated by glutamate acting primarily at AMPA/kainate receptors.

4. In the majority of cases, there was no correlation between the amplitude of EPSPs underlying each Gaussian and the EPSP rise time but there was a positive correlation between the EPSP half-width and EPSP rise time. The rise times of EPSPs underlying the first, and all, fitted Gaussians were similar to that for the total sample of EPSPs in each motoneurone. Taken together, this suggests that the EPSPs underlying each Gaussian arise from inputs to different dendritic compartments, and that the range of compartments is similar for EPSPs underlying successive Gaussians.

5. Two conclusions are drawn. First, EPSPs of different dendritic origin have similar amplitudes at the soma. Second, the multimodal distribution of EPSP amplitudes recorded in the presence of TTX raises the possibility that individual boutons may contain multiple release sites, with each perhaps operating on a separate functional group of postsynaptic receptors.

The present report stems from an unexpected finding made following use of the whole-cell patch method to record spontaneous EPSP activity in trigeminal motoneurones. Earlier *in vivo* (Grimwood, Appenteng & Curtis, 1992) and *in vitro* (Curtis & Appenteng, 1993) studies, involving use of conventional sharp electrodes to obtain simultaneous recordings from pairs of single neurones, had shown that excitatory transmission on trigeminal motoneurones can be accompanied by a high incidence of failures (i.e. presynaptic impulses failing to elicit detectable postsynaptic events). However, the sometimes rather poor signal-to-noise ratio obtained meant that some synaptic responses may have gone undetected, so possibly resulting in a significant overestimation of the incidence of failures.

Whole-cell patch recording offers an improved means of detecting synaptic responses and so we set out to use this method to obtain intracellular recordings from trigeminal motoneurones. A feature of these recordings was the presence of plentiful untriggered EPSP activity. Plots of the amplitude distributions of these EPSPs revealed the presence of clear equidistant peaks for almost all cells studied. An analysis of the half-widths and rise times of the EPSPs indicated that the EPSPs arose from inputs to different compartments of the dendritic tree and the implications of this are discussed. Preliminary accounts of this work have been presented to the Physiological Society (Curtis, Appenteng & Min, 1994*a*; Curtis, Min & Appenteng, 1994*b*).

METHODS

Preparation

This was as described in detail by Curtis & Appenteng (1993). In brief, rats aged 8 days were anaesthetized with a mixture of 5% halothane in oxygen and decapitated. The brain was exposed and longitudinal tissue slices (500 μm thick) which encompassed the trigeminal motor nucleus and surrounding regions were cut. Slices were placed in an interface-type chamber and perfused with ACSF maintained at 25 °C. The ACSF contained (mM): 105 NaCl, 5 KCl, 1·3 or 1·0 $MgSO_4$, 10 glucose, 24 $NaHCO_3$, 1·2 NaH_2PO_4, and 0·9 or 2·0 Ca^{2+}; pH adjusted to 7·4 by gassing with 95% O_2–5% CO_2. The flow rate in the bath was set at 1–2 ml min^{-1}. The following drugs were added to the ACSF: TTX (0·6 μM, Sigma), added either to the ACSF composed as described, or to ACSF containing no added Ca^{2+} but with the Mg^{2+} concentration raised to 2·2 mM; and 6-cyano-7-nitroquinoxaline-2-3-dione (CNQX; 10 μM; Tocris).

Recording in the motor nucleus

Whole-cell recordings were made using patch electrodes pulled from thin-filament glass of 1·2 mm o.d. (Clark Electromedical). The electrodes were filled with a solution containing (mM): 100 potassium gluconate, 10 EGTA, 5 $MgCl_2$, and 40 Hepes; and had resistances of 5–15 MΩ. Recordings were obtained using the 'blind patch' technique (Blanton, Lo Turco & Kriegstein, 1989). Electrodes were initially lowered to a depth of 50–100 μm in the motor nucleus while applying positive pressure. Following a 10 min period of stabilization, the positive pressure was removed. With the amplifier (Axopatch-1D) set in the voltage recording mode, current pulses were passed down the electrode and the series resistance control adjusted so that the voltage trace was continuous at the make-and-break of the artifacts. The amplifier was then set in the voltage clamp mode and the current responses to 1 mV voltage pulses continually monitored as the electrode was moved slowly through the tissue. A decrease in the amplitude of the recorded current response was taken to indicate proximity of a cell. Seals of at least 2 GΩ were then obtained by applying gentle suction and a steady voltage of −60 mV. Following the formation of a seal, the electrode capacitance transients were reduced by adjusting the capacitance compensation. Whole-cell recordings were then made by gently applying further suction with 'breakthrough' indicated by the appearance of large transients at the start and end of the pulse. All subsequent recordings were made with the amplifier in the voltage recording mode. The breakthrough to the whole-cell mode was accompanied by an increase in access resistance of the electrode, typically from a mean resistance of 6 MΩ to a mean of 47 MΩ (S.D. = 19; $n = 36$), necessitating a rebalancing of the bridge. Neurones were only accepted for further study if the seal resistance formed prior to 'breakthrough' was at least 2 GΩ, the membrane potential at least −60 mV and the spikes overshot 0 mV. Signals were low-pass filtered at a corner frequency of 2 kHz and then digitized on-line at a frequency of 10 kHz using a CED 1401 interface (Cambridge Electronic Design).

The neuronal input resistance (R_n) of neurones was determined from the peak averaged transmembrane response to hyperpolarizing current pulses of 200–400 ms duration (Fig. 1*B*). Depolarizing current pulses of 200 ms duration were used to determine rheobase (R_h) and 500 ms pulses for determination of the repetitive firing ability of neurones (Fig. 1*A*). Membrane time constants (τ_o) were determined from the averaged transmembrane response to 0·5 ms, 1 nA, hyperpolarizing current pulses (Fig. 1*C*: see Curtis & Appenteng, 1993).

EPSP activity was recorded in normal ACSF and the slices then continuously bathed in ACSF with added TTX. TTX application resulted in abolition of action potential propagation in the slice, as evidenced by the inability of all neurones to fire action potentials in response to depolarizing current pulses applied at intensities of three times that required to elicit repetitive firing. Recordings of EPSP activity were commenced some 10 min after block of action potential propagation.

Recording with conventional glass electrodes

Conventional sharp electrodes filled with 4 M potassium acetate were used to determine the membrane properties of motoneurones in normal ACSF. The recordings were made using a Neurolog DC amplifier and membrane properties determined as above. In some experiments the electrodes were filled with neurobiotin (2% neurobiotin in 2 M potassium acetate, pH = 7·4; Horikawa & Armstrong, 1988) to allow the determination of the electrical properties to be combined with the intracellular labelling of the motoneurone. Neurones were labelled by iontophoretic ejection of 8·25 nA min^{-1} of neurobiotin using depolarizing current pulses (duration, 0·15 s; cycle time, 0·3 s; repetition frequency, 3·3 Hz). Electrodes were left in the cells for a minimum of 5 min after the termination of filling, and slices left in the chamber for a further 30 min to 1 h before removal from the chamber. Slices were placed overnight in cold (4 °C) fixative consisting of 2% paraformaldehyde, 1·5% saturated picric acid and 1·25% glutaraldehyde in 0·1 M phosphate buffer (pH = 7·4). The slices were then washed overnight in 0·1 M phosphate buffer, embedded in 10% gelatine and serial sections (60 μm) were cut on a vibratome. The sections were incubated in 0·1% Triton X-100 in phosphate-buffered saline (PBS) for 30 min, followed by a 1 h incubation in 2% bovine serum albumin in PBS and then incubated overnight in an avidin–biotin–horseradish peroxidase conjugate (ABC reagent, Vector, CA, USA) at 4 °C. The horseradish peroxidase activity was visualized using diaminobenzidine as the chromogen and the reaction product intensified with cobalt.

Analysis of morphometric data

The neuronal morphology was reconstructed from camera lucida drawings made using a ×100 oil immersion lens (numerical aperture, 1·5) to view the sections, at a total magnification of ×1600. Measurements of diameter and length were made, as in the study of Curtis & Appenteng (1993) using a digitizing tablet (resolution, 0·01 mm). The diameters of all dendrites were measured at a minimum of three points along each dendritic segment and the mean value taken as the diameter of the dendritic segment. A pythagorean correction was used to correct all measurements of length for the effect of depth through the sections, and no correction was made for shrinkage induced by the histological procedures. Soma surface area was derived by approximating the soma to an ellipsoid. The mean lengths of dendrites were determined by taking the average of the individual path lengths from the soma to each dendritic termination. The path lengths were determined by summing the lengths of dendritic segments that lay along a path between the soma and the dendritic termination. There was no systematic variation of dendritic diameter between branch points and so the surface area of dendritic segments could be calculated by representing them as cylinders and their areas summed to give the complete dendritic surface area.

Rall (1959) has shown that impedance matching at branch points occurs when the summed diameters of daughter dendrites ($d_{daughter}$) raised to the 3/2 power equals the diameter of the parent dendrite (D_p) raised to the 3/2 power (i.e. $\Sigma(d_{daughter}{}^{3/2})/D_p{}^{3/2} = 1$).

This ratio was therefore determined at each branch point. The electrotonic length (L) of individual dendrites was calculated starting from:

$$L = l/\lambda.$$

The space constant (λ) is given by $\sqrt{(R_m/4R_i)d}$, where R_m is the specific membrane resistivity, R_i the specific cytoplasmic resistivity, and d the diameter of a dendritic segment. C_m (the specific membrane capacitance) was assumed to be 1 μF cm^{-2} and therefore R_m (Ω cm^2) assumed to equal τ_0 (ms). R_i was assumed to equal 100 Ω cm^{-1} (Rall, 1977). The value of L for the entire dendrite was obtained by taking the mean of the individual dendritic terminations.

Analysis of EPSPs recorded with patch electrodes

Positive-going events showing a single smooth rising phase, which was shorter than the decay phase, were assumed to be single EPSPs and measurements made of their amplitude (Fig. 1*D*; $a_p - O$), 20–80% rise time (Fig. 1*D*) and duration above half-amplitude (i.e. half-width). EPSPs showing an inflection on their rising phase were excluded from the analysis. The amplitude of the baseline noise preceding single EPSPs was determined by measuring the voltage at the start and end of a window, the duration of which was set to equal that of the time difference from the start to the peak of the EPSP (Fig. 1*D*; $a_n - O$). All measurements were made using semi-automatic routines written within the Spike2 software supplied by CED. Histogram plots were constructed of the amplitude distribution of single EPSPs. The distributions were examined at a minimum of three different bin widths to assess if the histograms showed peaks at consistent locations in the different plots. In cases where this criterion was satisfied, the position of peaks was then determined by fitting the unbinned amplitude data with a fit consisting of the sum of up to four Gaussians using the maximum likelihood procedure of Colquhoun & Sigworth (1983; see also Edwards, Konnerth &

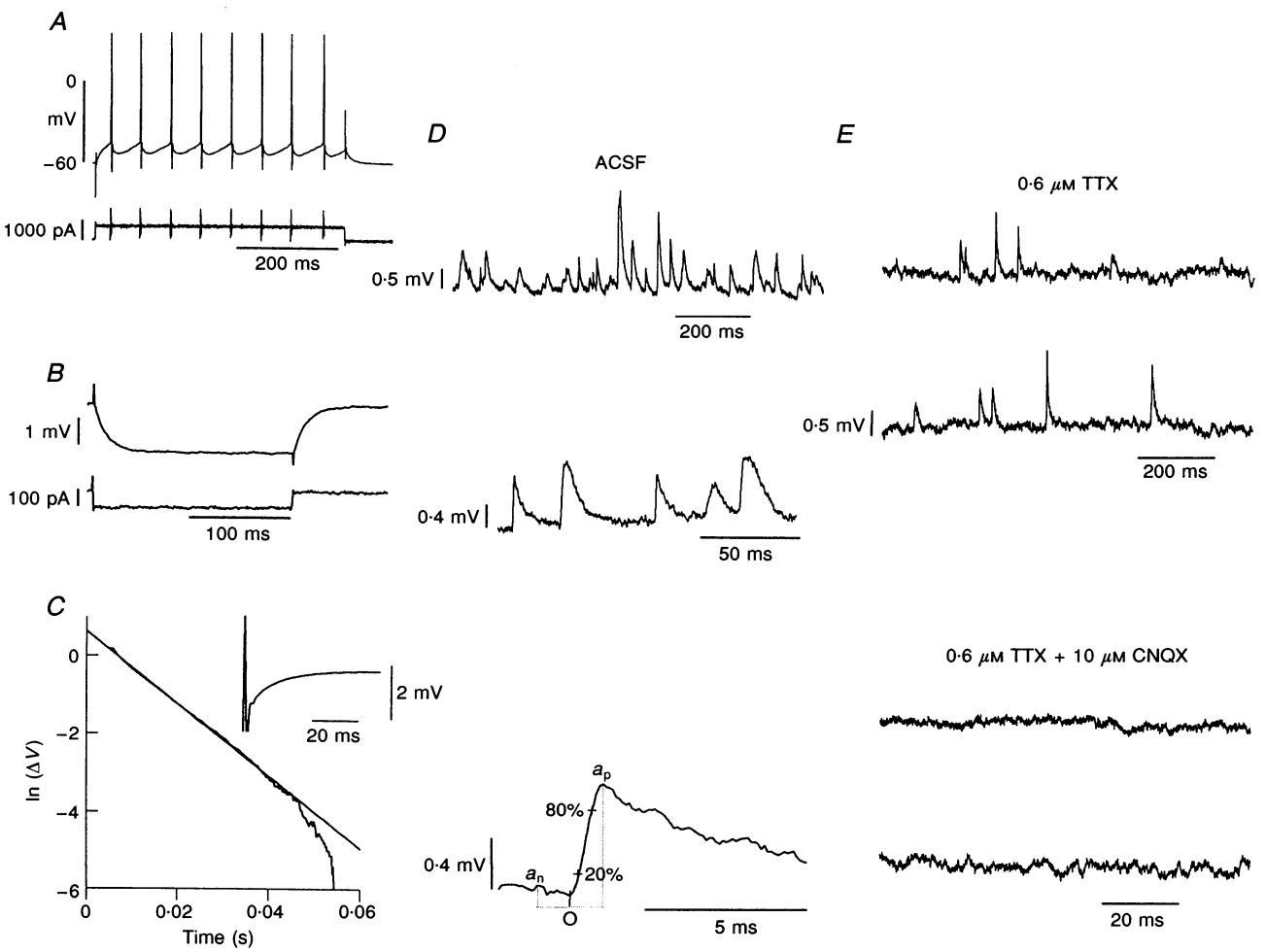

Figure 1. Whole-cell recording from trigeminal motoneurones

A, response of a motoneurone to a single depolarizing current pulse. *B*, averaged response of the neurone to a hyperpolarizing current pulse ($n = 32$ sweeps). *C*, semilogarithimic plot of the decay of the voltage response in a cell to injection of a 0·5 ms, 1 nA hyperpolarizing current pulse. Note that the first 5 ms of the voltage response after the onset of the current pulse has not been plotted. The continuous line shows the best fitted straight line to the data plotted. Membrane time constant is determined from the time taken for the voltage to decay to 1/e of its initial value. *D*, top panel shows sEPSP activity and lower panel measurements made on single EPSPs (see text; cell 7). *E*, effect of CNQX on mEPSP activity (cell 7).

Table 1. Membrane and spike properties of motoneurones determined with parch and sharp electrodes

	V_m (mV)	Spike amplitude (mV)	R_n (MΩ)	Rheobase (pA)	Time constant (ms)
Patch (8 days old)					
Mean	−64 ± 4 (36)	106 ± 16 (34)	161 ± 227 (36)	266 ± 314 (34)	8·62 ± 1·48 (10)
Range	−60 to −74	78–166	7·9–1026	10–1000	6·25–10·08
Sharp (8 days old)					
Mean	−66 ± 5·2 (45)	72 ± 7·4 (42)	13·5 ± 4·8 (45)	830 ± 490 (43)	3·41 ± 0·63 (8)
Range	−60 to −78	60–90	3·6–28·5	160–2630	2·6–4·1
Sharp (13 days old)					
Mean	−66 ± 5·4 (87)	77 ± 11 (87)	7·5 ± 2·5 (69)	1600 ± 1100 (56)	3·5 ± 2·2 (35)
Range	−60 to −81	60–115	2·6–14·7	300–6200	0·83–13·7
Probability (P)					
Patch *vs.* sharp	—	<0·001	<0·001	<0·001	<0·001
Sharp *vs.* sharp	—	<0·05	<0·05	<0·05	—

Mean values are means ± S.D. with the number of experiments given in parentheses. R_i, input resistance. Motoneurones used in patch *vs.* sharp comparison were from 8-day-old rats. Sharp *vs.* sharp comparisons were from 8- and 13-day-old rats. P determined by Student's t test.

Sakmann, 1990; Jonas, Major & Sakmann, 1993). As described by Edwards *et al.* (1990), the function maximized was

$$\log P = \sum_i \log\left(\sum_k A(k)\exp\left(-0{\cdot}5\left(\frac{Y(i)-M(k)}{\sigma_p(k)}\right)^2\right)\Big/\left(\sqrt{(2\pi)}\sigma_p(k)\right)\right),$$

where $Y(i)$ are the measured amplitude values, k is the incremental number of the Gaussian and $M(k)$ is the mean, $\sigma_p(k)$ is the S.D. and $A(k)$ the relative area under the Gaussian k. The decision as to the number of Gaussians to be fitted was based on visual inspection of the plots at different bin widths. The initial estimate of $\sigma_p(k)$ was based on the measured noise standard deviation but values of $\sigma_p(k)$ were then allowed to vary freely during the fitting. The fitted distributions were compared with the original binned distributions using a χ^2 statistic and fits accepted if they passed this test at the 95% confidence level or higher.

The mean separation between peaks in the fit to the unbinned data (q) was assessed, as described by Jonas *et al.* (1993), from

$$q = \frac{1}{n}\sum(M_{(k)}/k),$$

where n equals the total number of peaks in the fit. Peaks were judged to be equidistant if the standard deviation of the sum of the $M(k)/k$ values (Edwards *et al.* 1990) was less than 15% of q. EPSPs recorded in the presence of TTX are referred to as miniature EPSPs (mEPSPs) while EPSPs recorded in the absence of TTX are referred to as spontaneous EPSPs (sEPSPs).

RESULTS

Membrane properties determined with patch and sharp electrodes

Initial attempts to obtain whole-cell recordings from animals aged 13–15 days proved largely unsuccessful, with many seals being formed on apparent non-neuronal elements. The use of tissue slices from 8-day-old rats resulted in a considerable improvement in yield and so was adopted. Table 1 summarizes the data on the membrane and spike properties of motoneurones recorded with patch and sharp electrodes in animals aged 8 days. Values of R_n, R_h and spike amplitude obtained with patch electrodes varied independently of the access (i.e. electrode) resistance of the recording ($P > 0{\cdot}3$ in each case). The values of spike amplitude, R_n and τ_o determined using patch electrodes were significantly higher than those obtained with sharp electrodes, while R_h values determined with patch electrodes were significantly lower (Student's t test). Similar differences have been reported in comparisons of data obtained with patch and sharp electrodes in other systems (see Spruston & Johnston, 1992; Spruston, Jaffe & Johnston, 1994) and have been ascribed largely to the improved seal associated with patch recordings. Comparison of data obtained at 25 °C with sharp electrodes in animals aged 8 days and animals aged 13–15 days (Curtis & Appenteng, 1993) reveals a significant decrease in R_n and an increase in R_h.

Quantitative dendritic morphology of neurones

Quantitative morphological data was obtained from three motoneurones, recorded using conventional electrodes, in animals aged 8 days (Fig. 2*A*). The soma surface area of the neurones ranged from $0{\cdot}495 \times 10^3$ to $0{\cdot}806 \times 10^3$ μm^2. Each neurone had five primary dendrites and these branched up to eight times to produce a mean of 11·13 end-terminations per dendrite (S.D. = 6). The mean length of the dendrites was 472 μm (S.D. = 90) and the mean surface area of dendrites was $0{\cdot}62 \times 10^4$ μm^2 (S.D. = 0·35).

Table 2 summarizes the geometric data on motoneurones in animals aged 8 and 13 days, with the data from 13-day-old animals being taken from Curtis & Appenteng (1993). Motoneurones at 13 days have more primary dendrites (6–9) but the mean lengths of these dendrites, the number of end-terminations and the mean surface area of these dendrites were not significantly different from those in 8-day-old animals. The plots in Fig. 2*C* and *D* summarize the pattern of branching in 8- and 13-day-old animals. The lengths of dendritic segments in 13-day-old animals were generally

Table 2. Geometric data for motoneurones in 8- and 13-day-old rats

	Dendrites per neurone	Dendritic length (μm)	End-terminals per dendrite	Primary dendritic segment diameter (μm)	Dendritic surface area ($\times 10^4$ μm^2)	Surface area ratio* (%)	Neurone electrotonic length
8 days	5 (3)	472 ± 90 (15)	11·13 ± 6·00 (15)	3·18 ± 1·10 (15)	0·62 ± 0·35 (15)	97·2–98·7 (3)	1·54–1·81 (3)
13 days	6–9 (3)	552 ± 160 (22)	11·45 ± 8·75 (22)	3·01 ± 1·41 (22)	0·92 ± 0·67 (22)	98·3–99·2 (3)	1·38–2·20 (3)
P	—	0·086	0·848	0·692	0·12	—	—

Values are means ± S.D. with number of experiments in parentheses. * Surface area ratio is (total dendritic surface area)/(neuronal surface area). *P* determined by Student's *t* test.

longer than those of corresponding segments in 8-day-old animals but the differences were not statistically significant (Fig. 2*D*). The diameter of dendritic segments were, with the exception of the first two dendritic segments, significantly greater in 13-day-old animals (Fig. 2*E*). There was, at both ages, a linear relationship between the area of dendrites and the diameter of the stem (or primary) dendrite, with the slope of relationship being greater at 13- than at 8-days-old.

Electroanatomy of neurones

Figure 2*B* illustrates the distribution of the ratio $\Sigma(d_{daughter}^{3/2})/D_p^{3/2}$ for the three cells labelled in 8-day-old animals. The mean ratio for the total sample of branch points was 0·998 (S.D. = 0·29, $n = 149$), indicating that the condition required for impedance matching is met at most branch points and therefore that the three branches at each branch point can be collapsed into a single cylinder. The values of L, determined from the geometric data and a knowledge of the membrane time constant, were 1·54 (cell A; $\tau_0 = 2{\cdot}8$ ms), 1·81 (cell B; $\tau_0 = 2{\cdot}6$ ms) and 1·59 (cell C; $\tau_0 = 4{\cdot}1$ ms), with the mean value for the sample (1·65) being virtually identical to the mean value obtained in animals aged 13 days ($L = 1{\cdot}67$; Curtis & Appenteng, 1993). Thus, electrically, the dendritic trees at the two ages are of virtually identical mean length.

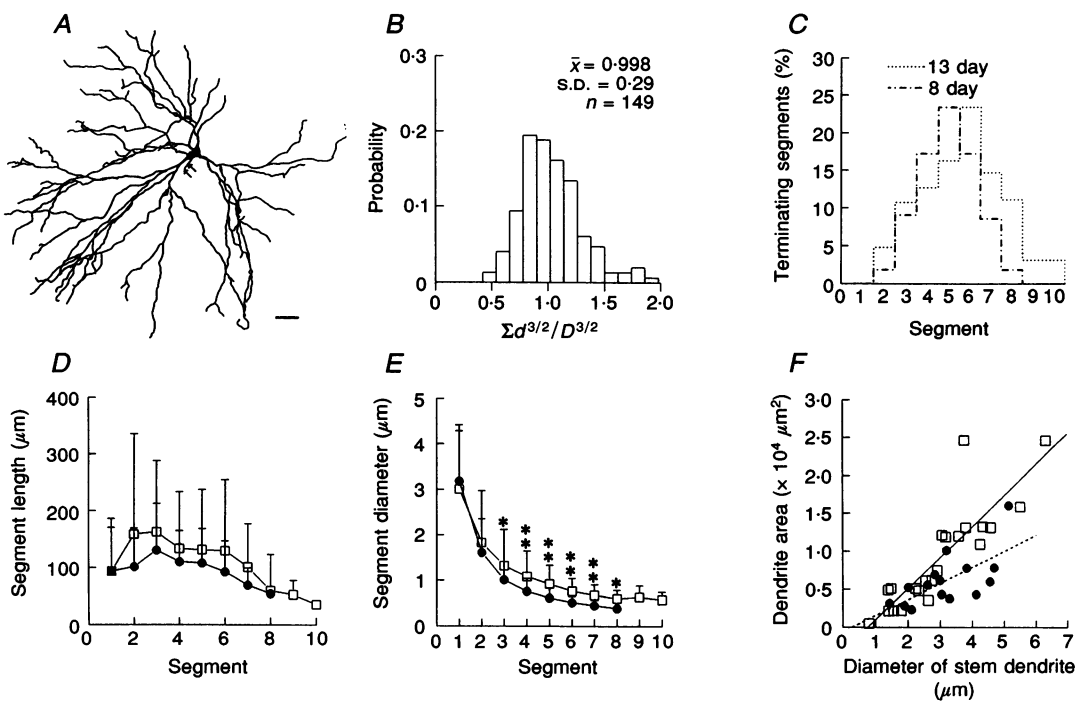

Figure 2. Quantitative morphology of motoneurones in animals aged 8 days

A, reconstructions of a motoneurone (cell 1). Scale bar = 50 μm. Arrows indicate axon. *B*, distribution of branch point ratios for all the total sample of motoneurones. *C*, proportion of of all segments forming end-terminations in each segment. The total number of end-terminations for the sample was determined and the percentages shown in the plot calculated. *D*, variation of mean (± S.D.) dendritic segment length with segment number. □, 13 days; ●, 8 days for this and following graphs. *E*, variation in mean diameter of dendritic segments. *F*, relationship between dendritic surface area and diameter of primary dendrite. Dashed line shows linear least square fit to data from 8-day-old animals (slope = 0·21, $P = 0{\cdot}006$) and continuous line the fit to data from 13-day-old animals (slope = 0·41, $P < 0{\cdot}001$).

Table 3. Measurement and fit parameters of EPSPs recorded from 8-day-old rats with patch electrodes

	R_n (MΩ)	Peak (μV) 1	2	3	4	5	q (μV)	Noise (μV)	Data points in fit/all	Amp (range) (μV)	Rise time (range) (ms)	Int (ms)
Cell 1												
sEPSP	39	n.f.	583 ± 101	993 ± 215	—	—	312 ± 27·6	37 ± 153	415/434	826 (238–2275)	0·64 ± 0·27 (0·26–2·54)	71
mEPSP		427 ± 112	758 ± 96	1123 ± 172	—	—	393 ± 29·1	23 ± 120	348/356	712 (190–2619)	0·65 ± 0·38 (0·2–5·11)	323
Cell 2												
sEPSP	43	340 ± 63	583 ± 148	1075 ± 161	—	—	330 ± 34·5	10 ± 50	266/270	514 (166–1611)	1·27 ± 0·70 (0·3–3·2)	222
mEPSP		310 ± 76	550 ± 130	895 ± 155	—	—	294 ± 17·8	−1·8 ± 41	169/175	541 (211–746)	1·25 ± 1·44 (0·22–5·29)	556
Cell 3												
sEPSP	31	240 ± 46	389 ± 59	572 ± 102	—	—	208 ± 27·4	12 ± 41	237/243	354 (158–1005)	0·92 ± 0·57 (0·2–3·14)	123
mEPSP		254 ± 47	417 ± 74	673 ± 98	—	—	229 ± 23·1	10 ± 38	281/285	383 (158–1031)	0·76 ± 0·48 (0·2–2·53)	208
Cell 4												
sEPSP	69	322 ± 56	590 ± 114	938 ± 116	—	—	310 ± 13·7	13 ± 96	324/354	633 (174–2095)	0·88 ± 0·43 (0·33–2·42)	333
mEPSP		399 ± 69	787 ± 144	1163 ± 116	—	—	393 ± 5·7	33 ± 87	251/330	940 (251–2671)	0·77 ± 0·25 (0·4–1·8)	370
Cell 5												
sEPSP	73	n.f.	585 ± 160	985 ± 204	1375 ± 224	1845 ± 270	333 ± 32	17 ± 166	267/281	1220 (264–3518)	1·73 ± 0·80 (0·35–4·83)	238
mEPSP		363 ± 85	661 ± 114	1050 ± 105	1515 ± 172	—	356 ± 20·4	11 ± 57	282/305	818 (185–3252)	1·60 ± 1·30 (0·32–6·21)	625
Cell 6												
sEPSP	180	307 ± 62	560 ± 117	913 ± 144	—	—	297 ± 14·9	29 ± 129	267/307	676 (185–3783)	6·02 ± 2·87 (1·7–13·8)	385
mEPSP		294 ± 54	504 ± 140	—	—	—	273 ± 29·7	9 ± 134	277/280	367 (169–867)	5·12 ± 2·60 (1·6–13·34)	400
0 Ca^{2+}		339 ± 56	571 ± 136	—	—	—	312 ± 37·8	16 ± 123	259/267	441 (211–2883)	4·65 ± 2·62 (1·1–13·8)	407
Cell 7												
sEPSP	40	n.f.	426 ± 99	667 ± 71	883 ± 51	1067 ± 139	217 ± 4·9	34 ± 58	406/445	869 (222–2730)	0·71 ± 0·45 (0·25–2·75)	63
mEPSP		n.f.	415 ± 81	620 ± 71	825 ± 98	1100 ± 140	210 ± 6·6	14 ± 60	352/367	737 (231–3136)	0·77 ± 0·52 (0·2–6·6)	303
0 Ca^{2+}		n.f.	438 ± 101	697 ± 87	892 ± 157	1121 ± 151	225 ± 5·6	15 ± 64	329/339	781 (202–4100)	0·76 ± 0·40 (0·3–2·39)	351

R_n, neuronal input resistance; q, mean spacing between peaks; Amp, amplitude; Int, interval between EPSPs; n.f., not fitted. Values are means ± S.D.

Amplitude distribution of EPSPs and noise

The synaptic activity recorded at potentials of around −60 mV consisted largely of EPSPs (Fig. 1*D* and *E*), but IPSPs could be seen on depolarization of the motoneurones. The amplitudes of the EPSPs detected ranged from 158 μV (cell 3; sEPSP and/or mEPSP) to 4100 μV (cell 7; 0 mM Ca^{2+}; Table 3) in different cells, with the mean amplitude of the EPSPs ranging from 354 μV (cell 3; sEPSPs) to 1220 μV (cell 5; sEPSPs: Table 3). On average, the ratio of the minimum EPSP amplitude and the noise standard deviation in individual cells was 3·3, a value similar to that reported by Jonas *et al.* (1993; see their methods and Table 1).

Figure 3*A*, *B* and *C* shows histogram plots of the noise and mEPSP amplitudes measured in two motoneurones. The plots are typical of the sample of motoneurones ($n = 9$) studied in that they show that while the noise distributions were unimodal and could be fitted by a single Gaussian, the distributions of mEPSP amplitudes were invariably 'peaky', with the peaks being evident at the same positions when the data was examined at a number of different bin widths (Fig. 3*A*). Peaks at similar positions were also seen when the data was divided into two equal subsets (Fig. 3*B*, $n = 178$ data points in each subset), though in the example shown in Fig. 3*B* the third peak seen in the plots of Fig. 3*A* could not be clearly resolved in the subsets. However, the observations

provide evidence that the peakiness may not just be a binning (e.g. Fig. 3*A*) or statistical artifact (Figs 3*B* and 4).

The continuous lines in Fig. 3*A* and *C* show the fits obtained using fits consisting of the sum of three Gaussians in Fig. 3*A* and four Gaussians in Fig. 3*C* (data points in fit given in Table 3). In each, the Gaussians are approximately equidistant, with the standard deviations of the peaks varying by only 7% of the mean spacing in Fig. 3*A* and by only 6% in Fig. 3*C*.

Figure 4*A–C* shows plots of the amplitude distribution of sEPSPs (*A*) and mEPSPs recorded in normal Ca^{2+} (*B*) and in 0 mM Ca^{2+} (*C*). The noise distribution in each plot was unimodal (not shown) while the distribution of sEPSPs and mEPSPs were peaky, with the position of the peaks being very similar in the three plots. The recordings in Fig. 4*A–C*, like those for cell 7 (see Table 3), were obtained over a period of some 45 min and so the presence of peaks in consistent positions provides further evidence that the peakiness may not simply be a statistical artifact associated with a finite sample.

Distributions showing peaks for both mEPSP and sEPSP activity were obtained for 9/9 motoneurones examined, with the peaks being equidistant for 7/9 motoneurones (see Table 3). The standard deviation of the individual Gaussians fitted was greater than the noise standard deviation for 39/50 Gaussians in Table 3, but the remaining eleven Gaussians had standard deviations less than that of the noise. Gaussians with standard deviations less than that of the noise have also been reported by Larkman, Stratford & Jack (1991) & Stricker, Field & Redman (1994) among others (see Jack, Larkman, Major & Stratford, 1994). For the

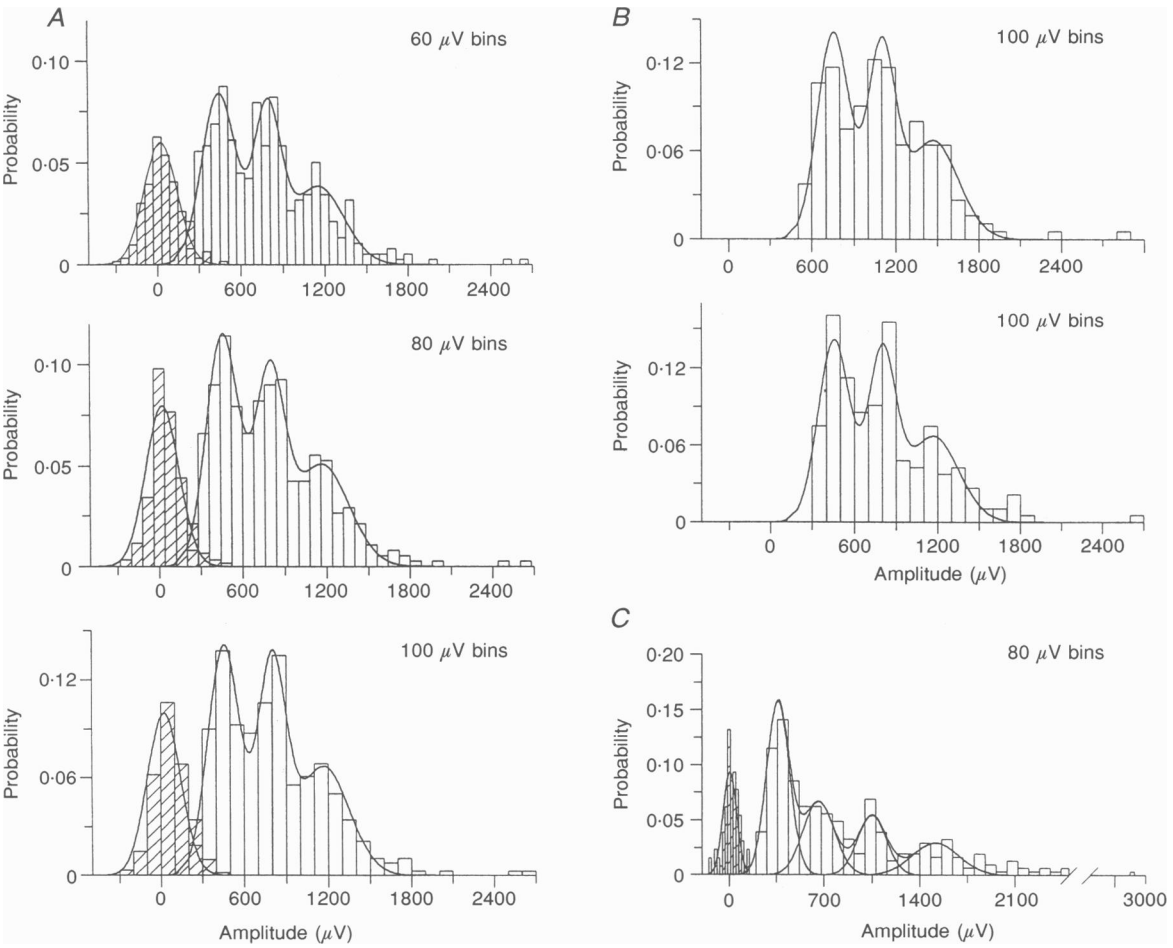

Figure 3. The peaky distribution of mEPSP amplitude

A, amplitude distributions of mEPSPs (□; $n = 356$) and noise (▨; cell 1). Continuous line shows fit to the distributions. *B*, amplitude distributions of first 178 (upper panel) and last 178 (lower panel) mEPSPs shown in *A*. Continuous line is the fit obtained to data in *A*. *C*, amplitude distribution of mEPSPs ($n = 305$) and noise recorded in another motoneurone (cell 5). Thin continuous lines show individual Gaussians fitted to the mEPSPs (□) and noise (▨), and thick continuous line the sum of the Gaussians fitted to the mEPSPs. Fit parameters of Gaussians (m = mean, subscripts refer to Gaussian number) in *A*: $m_1 = 427 \pm 112$ μV, $m_2 = 758 \pm 96$ μV, $m_3 = 1123 \pm 172$ μV; $q = 393 \pm 29$ μV; fit range = 190–1720 μV; data points in fit = 348. Fit parameters of Gaussians in *C*: $m_1 = 363 \pm 85$, $m_2 = 661 \pm 114$, $m_3 = 1050 \pm 105$; $m_4 = 1515 \pm 172$; $q = 356 \pm 20$; fit range = 185–1750 μV; data points in fit = 282.

thirteen histograms which involved fits to more than two peaks, plots were constructed of the variance of the individual Gaussians in a fit against peak number. With just one exception (cell 2; sEPSPs; $P = 0{\cdot}01$), no significant linear relationship was obtained between variance and peak number, suggesting an absence of a systematic change in variance of successive peaks.

Transmitter and receptors mediating EPSPs

Evidence as to the transmitter mediating the EPSPs was obtained by examining the effect of CNQX on the mEPSP activity. Bath application of a 10 μM dose of CNQX ($n = 4$) completely abolished all mEPSP activity (Fig. 1*E*). This suggests that the mEPSPs are all mediated by glutamate, with the glutamate acting primarily at AMPA/kainate receptors.

m/sEPSP amplitude and rise time

A feature of the data was that the rise times of both mEPSPs and sEPSPs recorded in individual neurones spanned a large range of values (Table 3). Figure 5 shows plots of amplitude and rise times for mEPSPs (Fig. 5*A b–A d*) and sEPSPs (Fig. 5*B b–B d*) underlying each of the Gaussians fitted to the data from a motoneurone (cell 3). In each case, there was no significant correlation between either mEPSP amplitude and rise time (Fig. 5*A b–A d*) or sEPSP amplitude and rise time (Fig. 5*B b–B d*) for EPSPs underlying each Gaussian fitted to the data. In addition, the rise times of EPSPs underlying the first, or all Gaussians, covered a similar range as EPSPs comprising the total sample (e.g. Fig. 5*A b–A d* and *B b–B d*).

Plots of the amplitudes of all mEPSPs obtained within individual neurones revealed no significant relationship between mEPSP amplitude and rise time for 6/7 cells in Table 3 (e.g. Figs 5*A a*, 6*A* and *C*). The one exception was cell 6 for which significant positive correlations were obtained between EPSP amplitude and rise time for each of the two Gaussians fitted to the mEPSP data and for one (the first) of the three Gaussians fitted to the sEPSP data. In contrast, plots of all sEPSPs obtained within individual neurones revealed positive correlations between sEPSP amplitude and rise time (e.g. Fig. 6*B* and *D*) for all bar cell 3 (Fig. 5*B a*).

m/sEPSP half-width and rise time

Values of the rise time of EPSPs recorded in a neurone are governed by the location of the synaptic input along the dendritic cable and by the time course of synaptic current injection. On the assumption of a similar time course for synaptic current injection at all synapses on a motoneurone, differences in rise time of EPSPs recorded within a neurone

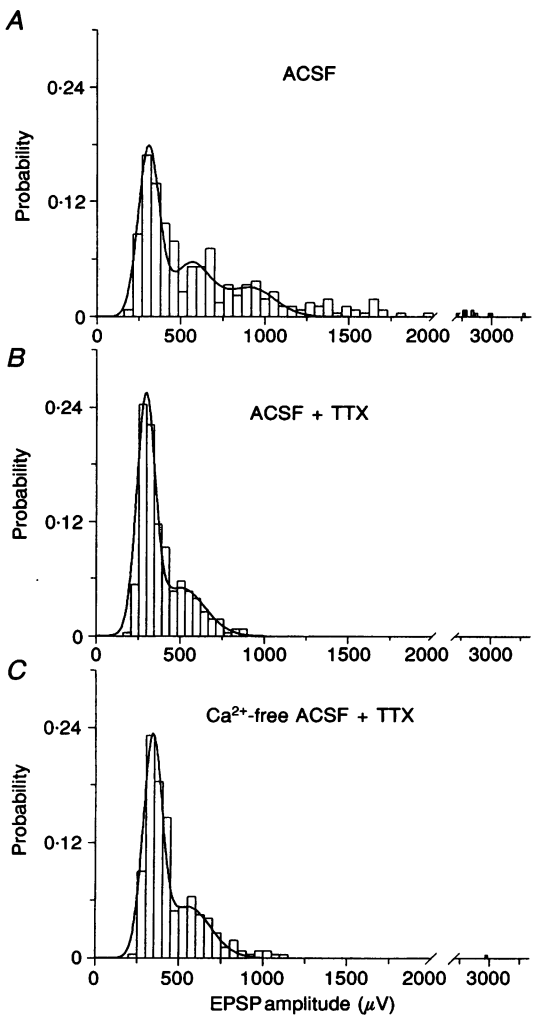

Figure 4. The effect of Ca^{2+} on the peaks of distribution of EPSP amplitude

Amplitude distributions of sEPSPs (*A*; $n = 307$ data points) and mEPSPs (*B*, $n = 280$; *C*, $n = 267$) recorded in a motoneurone (cell 6). Fit parameters (μV) in *A*: $m_1 = 307 \pm 62$, $m_2 = 560 \pm 117$, $m_3 = 913 \pm 144$; $q = 297 \pm 15$; fit range = 185–1220 μV; data points in fit = 267. Fit parameters (μV) in *B*: $m_1 = 294 \pm 54$, $m_2 = 504 \pm 140$; $q = 273 \pm 30$; fit range = 169–780 μV; data points in fit = 277. Fit parameters (μV) in *C*: $m_1 = 339 \pm 56$, $m_2 = 571 \pm 136$; $q = 312 \pm 38$; fit range = 211–873 μV; data points in fit = 259.

can be taken to reflect spatial differences in the location of the synapses along the dendritic tree (Jack & Redman, 1971; Jack, Noble & Tsien, 1975; Major, 1993). Under these circumstances, a general result from application of cable theory is that there should be a positive relationship between the EPSP half-width and the EPSP rise time (Jack & Redman, 1971). However, an alternative model is that the inputs may all be to the same compartment of the dendritic cable but the variations in the rise time of EPSPs may simply be a consequence of differences in the time course of synaptic current injection at different synapses. Jack & Redman (1971; see also Major, 1993) have shown in simulation studies that at any given location, variations in the time course of synaptic current injection alter EPSP rise time relatively much more than EPSP half-width, resulting in a wide range of EPSP rise times for each value of half-width (see chapter 7 of Jack *et al.* 1975). Plots of EPSP half-width and rise time can thus be used to distinguish between the above two possibilities.

We analysed the relationship between EPSP half-width and rise time for the six motoneurones (i.e. all bar cell 6) in which there was no correlation between m/sEPSP amplitude and rise time. For these six motoneurones there was a significant positive relationship between m/sEPSP half-width and rise time for the m/sEPSPs underlying each Gaussian fitted to the data (Fig. 5*Af–Ah* and *Bf–Bh*), with values of the slopes of the best fitted straight lines ranging from 1·9 to 5·5. The clear positive correlations obtained between m/sEPSP half-width and rise time support the suggestion that the m/sEPSPs underlying each Gaussian arise from inputs to different compartments of the dendritic cable.

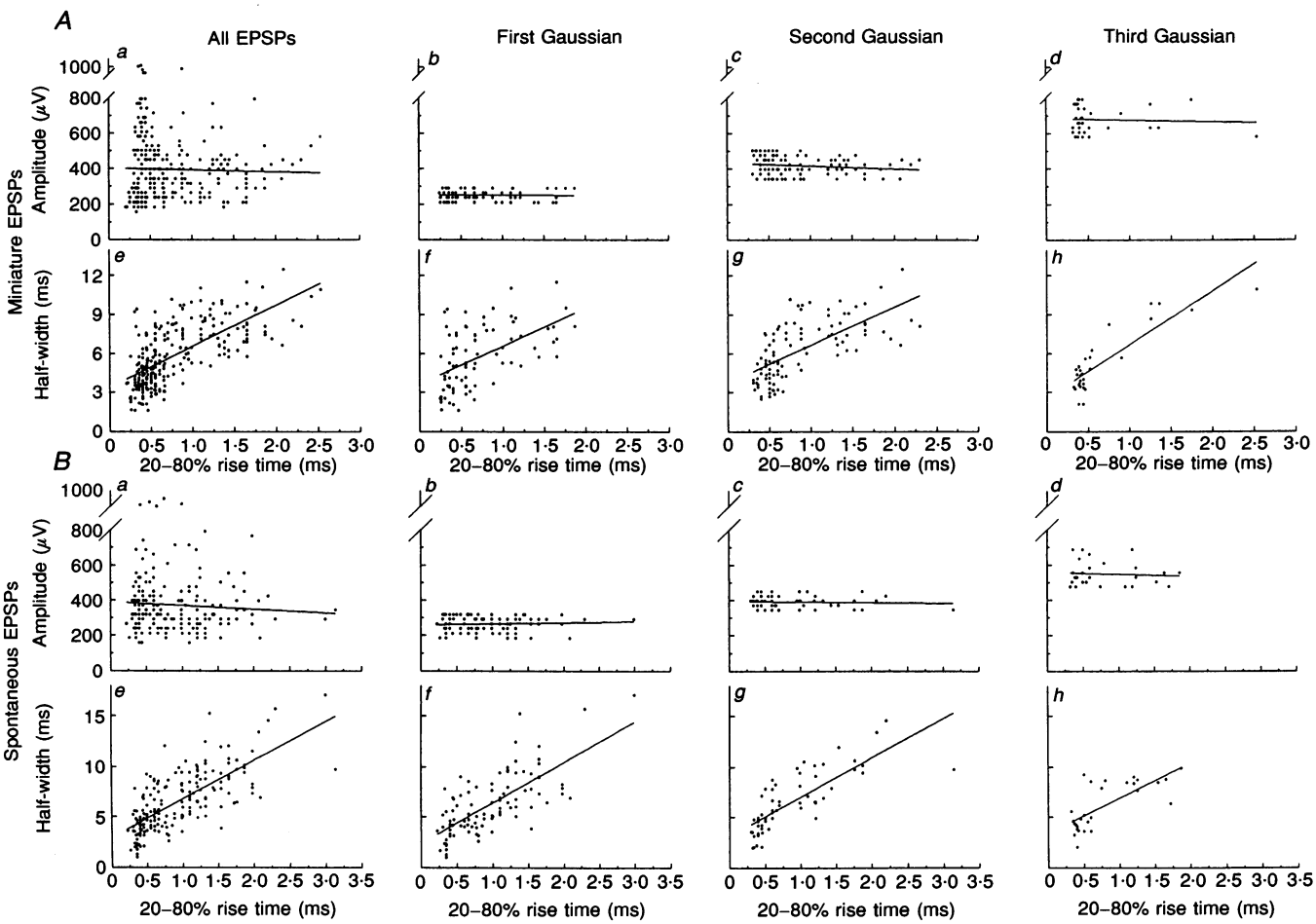

Figure 5. EPSPs of different dendritic origin have similar amplitudes when recorded at the soma

Amplitudes, half-widths and rise times of mEPSPs (*A*) and sEPSPs (*B*) recorded in the same motoneurone (cell 3). *Aa* and *Ba* show plots of the amplitude and rise time for all mEPSPs (*Aa*) and sEPSPs (*Ba*) recorded in the cell, and *Ae* and *Be* the corresponding plots of mEPSP (*Ae*) and sEPSP (*Be*) half-width and rise time. The upper panels in *A* and *B* show plots of the amplitude against rise time for mEPSPs (*Ab–d*) and sEPSPs (*Bb–d*) with amplitudes within one standard deviation of the mean of the first (*Ab* and *Bb*), second (*Ac* and *Bc*) and third Gaussian (*Ad* and *Bd*) fitted to the data. The lower panels in *A* and *B* show equivalent plots for the half-width and rise time for mEPSPs (*Af–h*) and sEPSP (*Bf–h*) underlying each Gaussian. The linear regression fit is superimposed on the individual plots. Values of correlation coefficent (r) for the individual plots were not significant for the plots in *Aa–d* and *Ba–d* ($P > 0{\cdot}05$), but were significant in *Af–h* and *Bf–h* ($P < 0{\cdot}001$).

DISCUSSION

The main findings of this study are that plots of the amplitude distribution of m/sEPSPs recorded in trigeminal motoneurones show clear, equally spaced, peaks. The m/sEPSPs underlying each peak have a broad range of rise times, and for the majority of cells, the m/sEPSPs underlying each peak arise from inputs to different parts of the dendritic cable.

Our evidence for the inputs arising from different parts of the dendritic cable is based on the observation of clear positive correlations between m/sEPSP half-width and rise time for m/sEPSPs underlying individual Gaussians. Thus, our data suggests that excitatory inputs to different parts of the dendritic cable can elicit m/sEPSPs of similar amplitude at the soma. This echoes earlier findings for synapses of single hindlimb muscle spindle afferents on to cat hindlimb motoneurones (Iansek & Redman, 1973; Jack, Redman & Wong, 1981) and for synapses of single vestibulospinal tract fibres on to hindlimb motoneurones (Harrison, Jack & Kullmann, 1989). The observation in each of these studies was that synapses located on different parts of the dendritic cable could elicit events of similar quantal amplitude at the soma (Iansek & Redman, 1973; Jack *et al.* 1981). Thus, a uniformity of EPSP amplitudes for inputs on to different parts of the dendritic cable may be a general feature of the integrative properties of somatic motoneurones. Motoneurones may be unique in this regard as similar behaviour has not been reported in other mammalian CNS neurones.

Iansek & Redman (1973) and Jack *et al.* (1981) proposed that the uniformity of EPSP amplitude in motoneurones could be explained on the basis of the motoneurones having a mechanism for ensuring a scaling of synaptic current at synapses on different parts of the dendritic tree. The mechanism(s) underlying the scaling were suggested to involve either a progressive alteration, with distance along the dendritic tree, in the postsynaptic density of receptors at excitatory synapses on the motoneurone, or a change in the unit conductance of receptors (i.e. receptor subtypes) on the different portions of the motoneurone dendritic tree (Iansek & Redman, 1973; Jack *et al.* 1981).

The above suggestion derived from recordings of EPSP activity and estimates of the electrical length of motoneurones made using conventional sharp electrodes. Use of patch electrodes has been found to result in higher estimates of membrane time constants, and thus shorter estimates of the electrotonic length of neurones (see Spruston *et al.* 1994). This has led to the realization that neurones may be more electrically compact than indicated by data obtained using conventional sharp electrodes, which in turn has sparked some debate as to just how much synaptic signals are attenuated by the dendritic tree of neurones. The propagation of potentials in dendritic cables is very frequency

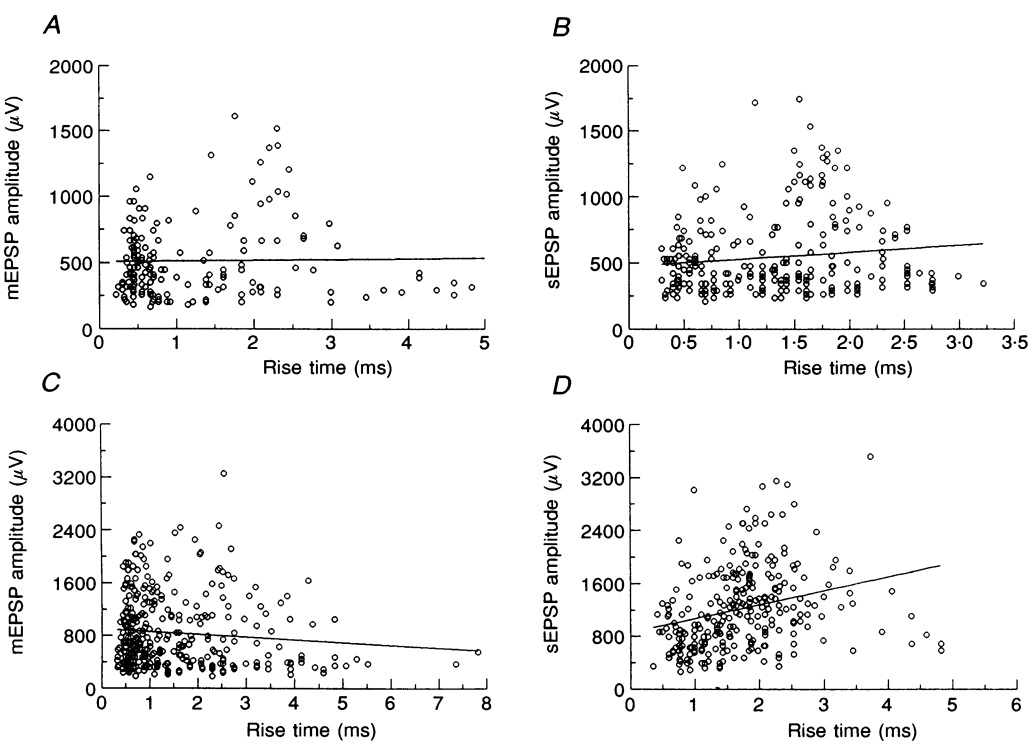

Figure 6. The relationship between EPSP amplitude and rise time

Data from two motoneurones (*A* and *B*, cell 2; *C* and *D*, cell 5). *A* and *C*, plots of mEPSP amplitude and rise time for all mEPSPs recorded in the two cells. *B* and *D*, similar plots for all sEPSPs recorded. The regression coefficients in *A* and *C* were not significant but were in *B* ($P = 0{\cdot}04$) and *D* ($P < 0{\cdot}001$).

dependent, with faster events being attenuated more than slower or steady-state events (see Jack *et al.* 1975; Spruston *et al.* 1994). Recent modelling studies on hippocampal neurones, with mean electrotonic lengths of 0·5, has shown that while attenuation of step inputs may only be nominal, fast synaptic inputs may show a 35–45% attenuation in amplitude (Spruston *et al.* 1994). Thus, as emphasized by Spruston *et al.* (1994), significant attenuation of synaptic signals can occur even in neurones which would be judged to be very electrically compact.

We found the membrane time constants obtained with patch electrodes to be 2·5 times higher than values obtained with sharp electrodes (Table 1). Recalculation of the electrotonic lengths of the neurones using estimates of membrane time constant increased by 2·5 times yields a revised estimate of 1·04 for the mean electrotonic length of the neurones to be expected using patch electrodes. Modelling studies on spinal motoneurones with electrotonic lengths of 1·0 suggest that fast synaptic inputs on the distal parts of the dendritic cable may be attenuated by some 80% in amplitude when recorded at the soma (see Fig. 7.27 of Jack *et al.* 1975; see also Harrison *et al.* 1989). Thus, significant attenuation of fast synaptic inputs may occur in the dendritic tree of trigeminal motoneurones in 8-day-old animals.

The observations in the present study of positive correlations between m/sEPSP half-width and rise time, peaks in the distribution of m/sEPSPs, and the absence of a correlation in most cells between mEPSP amplitude and rise time are all compatible with the suggestion of a scaling mechanism. In addition, the electrical length of the dendritic cable is compatible with there being significant attenuation of fast synaptic inputs on diffenent parts of the dendritic cable. However, these observations are not sufficient to prove the hypothesis of a scaling mechanism. Testing of the hypothesis will ultimately require determination of the distribution, and density, of glutamate receptor subtypes along the dendritic tree of the motoneurones, as well as development of a specific cable model of trigeminal motoneurones.

Quantal organization of transmission at synapses on trigeminal motoneurones?

The observations of consistent, equidistant, peaks in the amplitude distribution of both sEPSPs and mEPSPs, coupled with the finding of a unimodal distribution of the noise does provide the first suggestion that transmission at synapses on trigeminal motoneurones may be quantally organized as at other excitatory synapses in the CNS (see Jack *et al.* 1981; Konnerth, Keller & Lev-Tov, 1990; Larkman *et al.* 1991; Kullmann & Nicoll, 1992; Jonas *et al.* 1993). Here our argument is essentially similar to that employed by Liu & Feldman (1992) who observed, in phrenic motoneurones, peaks in the distributions of both sEPSCs and mEPSCs and suggested that this was compatible with a quantal organization of transmission. A number of authors have suggested that there may be little quantal variability at central excitatory synapses, with one piece of evidence cited being that fits to amplitude histograms of EPSPs and/or EPSCs can be obtained using models that assume a similar variance for all peaks in a fit (e.g. Jack *et al.* 1981; Redman, 1990; Larkman *et al.* 1991; Stricker *et al.* 1994; Jack *et al.* 1994). The absence, for the majority of our histograms, of a significant relationship between variance and peak number would suggest that there may also be little quantal variability at excitatory synapses on trigeminal motoneurones.

Peaky distribution of mEPSPs

Peaky distributions of miniature excitatory postsynaptic currents (mEPSCs) have been reported both for motoneurones (Liu & Feldman, 1992; Ulrich & Luscher, 1993) and a variety of other neurone types in the CNS (see Jonas *et al.* 1993; see also Edwards *et al.* 1990, for IPSCs). However, the analysis has been restricted to EPSCs with fast rise times because of the problems associated with obtaining an adequate space clamp of inputs away from the soma (Major, 1993; Spruston *et al.* 1994). The peaky miniatures have been attributed to a variety of factors which have included a contribution of inputs from different compartments, and a co-operativity or coupling of the release process at boutons. Our data indicates that mEPSPs underlying each peak arise from a range of dendritic compartments and so we can exclude the possibility that the separate peaks in the distributions of mEPSP amplitudes arise from activity in separate populations of boutons clustered at discrete compartments of the dendritic tree.

Thus, the peaky distributions must either be due to a coupling of the release from different boutons, or of the release process within single boutons. The key piece of information required, and which is lacking, concerns the number of functional release sites and the number of functional groups of postsynaptic receptors at boutons. Among the possibilities are that individual boutons contain a single functional release site operating on a single functional group of postsynaptic receptors (Jack *et al.* 1981), or alternatively that individual boutons contain a number of separate release sites each operating on a separate functional group of postsynaptic receptors (Edwards *et al.* 1990; Walmsley, 1991; Korn, Bausela, Charpier & Faber, 1993; Korn, Sur, Charpier, Legendre & Faber, 1994).

A coupling of the release from different boutons would require there to be mechanisms which, in the absence of action potentials, could act to couple release from different boutons. Any asynchrony in the coupling of release from different boutons would be expected to result in larger events having slower rise times and this would be evident as a positive correlation between mEPSP amplitude and rise time. Positive correlations were obtained for sEPSPs, where differences in propagation time of action potentials down the different collaterals of individual presynaptic neurones terminating on a motoneurone may have produced some asynchrony of release. However, the crucial observation was that for the majority of cells, no correlation was obtained between mEPSP amplitude and rise time when considering

all mEPSPs recorded in individual cells. This suggests that the peaky distribution of mEPSP amplitudes may not simply stem from a coupling of the release from different boutons.

We are thus left with the possibility that the coupling may be of the release process occurring within individual boutons. Jack *et al.* (1994) have discussed the possibility that spontaneous fluctuations in intraterminal calcium could, in the absence of action potentials, produce a synchronization of release from different sites within the same bouton. This raises the intriguing possibilities that individual boutons may not necessarily act as single functional units, and that physiological regulation of the mechanisms acting to couple release from different sites within a bouton may provide a powerful presynaptic mechanism for modifying the efficacy of synaptic transmission.

Blanton, M. G., LoTurco, J. J. & Kriegstein, A. R. (1989). Whole cell recording from neurons in slices of reptilian and mammalian cerebral cortex. *Journal of Neuroscience Methods* **30**, 203–210.

Colquhoun, D. & Sigworth, F. J. (1983). Fitting and analysis of single-channel records. In *Single Channel Recording*, ed. Sakmann, B. & Neher, E., pp. 191–263. Plenum Press, New York.

Curtis, J. C. & Appenteng, K. (1993). The electrical geometry, electrical properties and synaptic connections onto rat V motoneurones *in vitro*. *Journal of Physiology* **465**, 85–119.

Curtis, J. C., Appenteng, K. & Min, M.-Y. (1994*a*). Evidence for quantal transmission at excitatory synapses on to rat trigeminal motoneurones *in vitro*. *Journal of Physiology* **479.P**, 43*P*.

Curtis, J. C., Min, M.-Y. & Appenteng, K. (1994*b*). Whole-cell patch recordings from rat trigeminal motoneurones *in vitro*. *Journal of Physiology* **476.P**, 75*P*.

Edwards, F. A., Konnerth, A. & Sakmann, B. (1990). Quantal analysis of inhibitory synaptic transmission in the dentate gyrus of rat hippocampal slices: a patch-clamp study. *Journal of Physiology* **430**, 213–249.

Grimwood, P. D., Appenteng, K. & Curtis, J. C. (1992). Monosynaptic EPSPs elicited by single interneurones and spindle afferents in trigeminal motoneurones of anaesthetized rats. *Journal of Physiology* **455**, 641–662.

Harrison, P. J., Jack, J. J. B. & Kullmann, D. M. (1989). Monosynaptic EPSPs in cat lumbosacral motoneurons from group Ia afferents and fibres descending in the spinal cord. *Journal of Physiology* **412**, 43–63.

Horikawa, K. & Armstrong, W. E. (1988). A versatile means of intracellular labelling: injection of biocytin and its detection with avidin congugates. *Journal of Neuroscience Methods* **25**, 1–11.

Iansek, R. & Redman, S. J. (1973). The amplitude, time course and charge of unitary excitatory postsynaptic potentials evoked in spinal motoneurones and dendrites. *Journal of Physiology* **234**, 665–688.

Jack, J. J. B., Larkman, A. U., Major, G. & Stratford, K. J. (1994). Quantal analysis of the synaptic excitation of CA1 hippocampal pyramidal cells. *Advances in Second Messenger and Phosphoprotein Research* **29**, 275–299.

Jack, J. J. B., Noble, D. & Tsien, R. W. (1975). *Electric Current Flow in Excitable Cells*. Clarendon Press, Oxford.

Jack, J. J. B. & Redman, S. J. (1971). The propagation of transient potentials in some linear cable structures. *Journal of Physiology* **215**, 283–320.

Jack, J. J. B., Redman, S. J. & Wong, K. (1981). The components of synaptic potentials evoked in cat spinal motoneurones by impulses in single group Ia afferents. *Journal of Physiology* **321**, 65–96.

Jonas, P., Major, G. & Sakmann, B. (1993). Quantal analysis of unitary EPSCs at the mossy fibre synapse on CA3 pyramidal cells of rat hippocampus. *Journal of Physiology* **472**, 615–663.

Konnerth, A., Keller, B. U. & Lev-Tov, A. (1990). Patch clamp analysis of excitatory synapses in mammalian spinal cord slices. *Pflügers Archiv* **417**, 285–290.

Korn, H., Bausela, F., Charpier, S. & Faber, D. S. (1993). Synaptic noise and multiquantal release at dendritic synapses. *Journal of Neurophysiology* **70**, 1249–1254.

Korn, H., Sur, C., Charpier, S., Legendre, P. & Faber, D. S. (1994). The one-vesicle hypothesis and multivesicular release. *Advances in Second Messenger and Phosphoprotein Research* **29**, 301–322.

Kullmann, D. M. & Nicoll, R. A. (1992). Long-term potentiation is associated with increases in quantal content and quantal amplitude. *Nature* **357**, 240–244.

Larkman, A., Stratford, K. & Jack, J. J. B. (1991). Quantal analysis of excitatory synaptic action and depression in hippocampal slices. *Nature* **350**, 344–347.

Liu, G. & Feldman, J. L. (1992). Quantal synaptic transmission in phrenic motor nucleus. *Journal of Neurophysiology* **68**, 1468–1472.

Major, G. (1993). Solutions for transients in arbitrarily branching cables: III. Voltage clamp problems. *Biophysical Journal* **65**, 469–491.

Redman, S. J. (1990). Quantal analysis of synaptic potentials in neurons of the central nervous system. *Physiological Reviews* **70**, 165–198.

Spruston, N., Jaffe, D. B. & Johnston, D. (1994). Dendritic attenuation of synaptic potentials and currents: the role of passive membrane properties. *Trends in Neurosciences* **17**, 161–166.

Spruston, N. & Johnston, D. (1992). Perforated patch-clamp analysis of the passive membrane properties of three classes of hippocampal neurons. *Journal of Neurophysiology* **67**, 508–529.

Stricker, C., Field, A. C. & Redman, S. J. (1994). Probabilistic secretion of quanta at excitatory synapses on CA1 pyramidal neurons. *Advances in Second Messenger and Phosphoprotein Research* **29**, 323–340.

Ulrich, D. & Luscher, H.-R. (1993). Miniature excitatory synaptic currents corrected for dendritic cable properties reveal quantal size and variance. *Journal of Neurophysiology* **69**, 1769–1773.

Walmsley, B. (1991). Central synaptic transmission: studies at the connection between primary afferent fibres and dorsal spinocerebellar tract (DSCT) neurones in Clarke's column of the spinal cord. *Progress in Brain Research* **36**, 391–423.

Acknowledgements

The work was supported by The Wellcome Trust. Some of the experiments were performed with John C. Curtis. We thank Malcolm Hunter for the introduction to patching, and John Curtis, Dimitri M. Kullmann, Alan U. Larkman, and Guy Major for helpful comments on the manuscript.

Received 26 January 1995; accepted 17 February 1996.